Supporting Information (SI)

Chiral Resolution of DL-Leucine via Tartaric Acid Derivatives Salifying

Linlin Shi,[a] Zhiqiang Guo,[b] Xiaofang Luo,[a] Lingli Hou,[a] Hongchang Wu,[a] Ruiyu De,[a] Xin Huang,[a] Ting Wang,[a] Hongxun Hao,[a] Na Wang *[a] and Lina Zhou *[a]

[a]National Engineering Research Center of Industrial Crystallization Technology, School of Chemical Engineering and Technology, Tianjin University, Tianjin, 300072, People's Republic of China

[b]Jewim Pharmaceutical (Shandong) Co., Ltd., Shandong, 271000, People's Republic of China

*Corresponding Author

Email: linazhou@tju.edu.cn; wangna224@tju.edu.

Contents

the separation effect.

Fig. S7. HPLC data of the collected solids and liquids in each cycle.

Table S1. FT-IR stretching/bending vibration frequencies of D-/L-LEU, D-DTTA, the slurry product of D-LEU with D-DTTA and the slurry product of L-LEU with D-DTTA.

Table S2. Crystallographic parameters of the prepared salts.

Table S3. Hydrogen-bond metrics in crystal structures.

Table S4. The mole fraction solubility of D-D and L-D from 10 ℃ to 40 ℃ (p=101.3 kPa).

Table S5. Atomic topological path parameters at bond critical points in D-D.

Table S6. Atomic topological path parameters at bond critical points in L-D.

Table S7. Binding energies of D-DTTA with chiral LEU molecules.

Table S8. Solvation Free Energy of D-D and L-D.

Screening of experimental conditions for resolution:

Specific conditions of multiple cycle crystallization process:

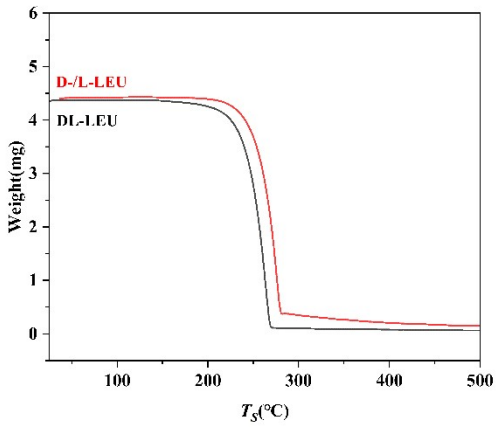

Fig. S1. TGA curves of DL-LEU and D-/L-LEU.

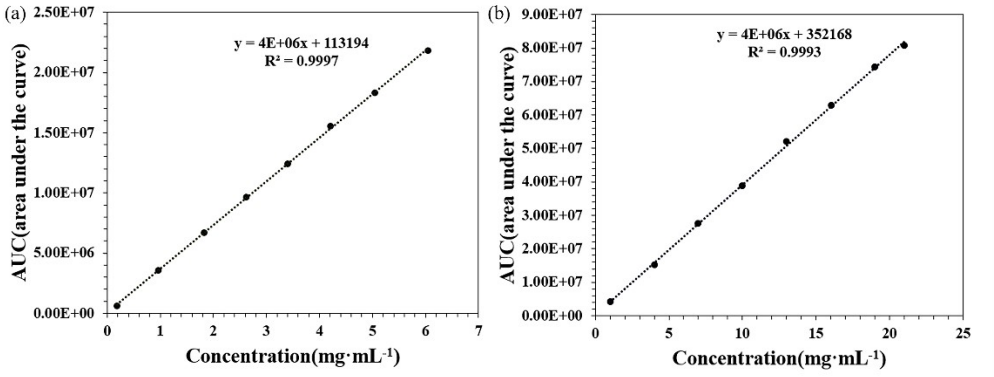

Fig. S2. The standard solubility curves of (a) D-D and (b) L-D.

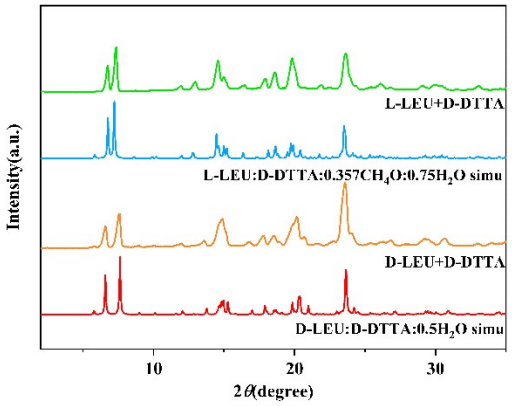

Fig. S3. PXRD spectra of D-D and L-D.

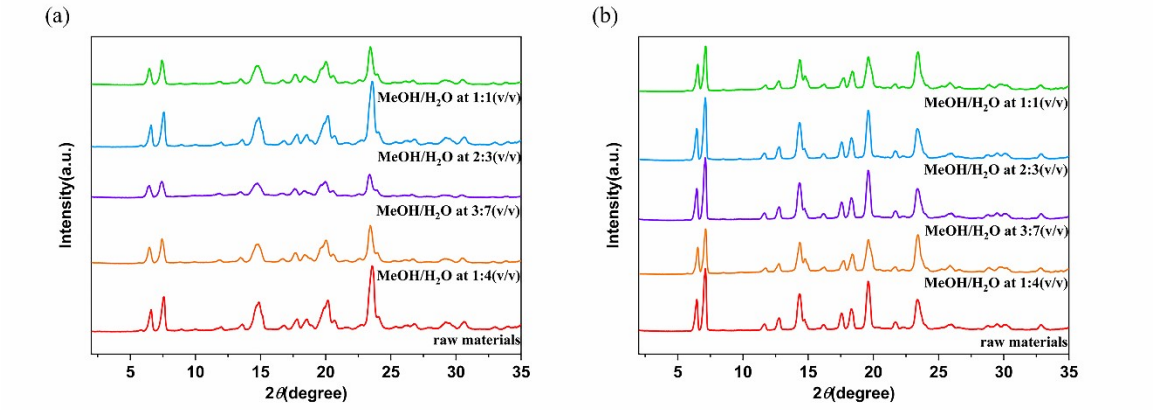

Fig. S4. PXRD spectra after solubility determination (a)D-D and (b)L-D.

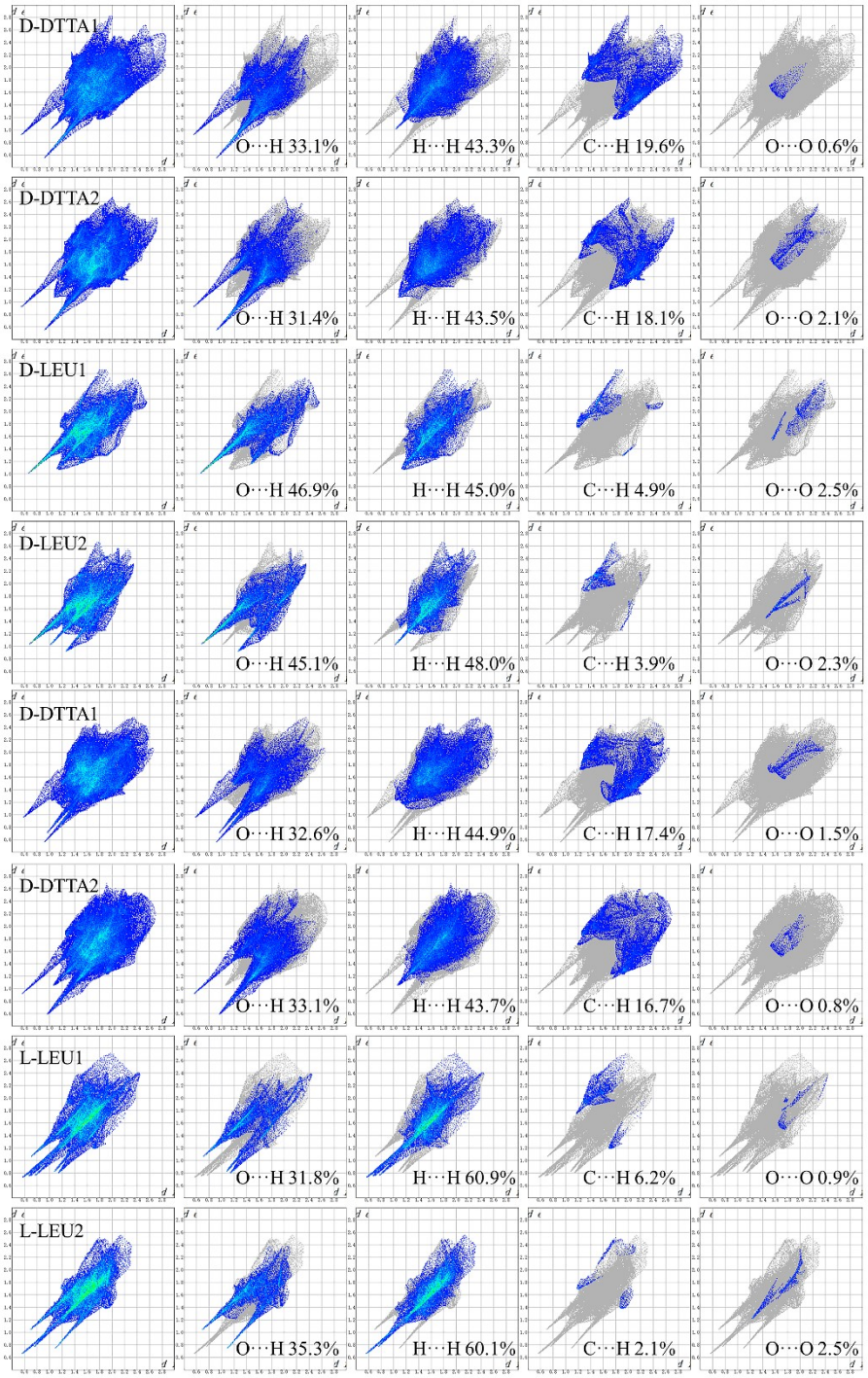

Fig. S5. 2D fingerprints of different contacts in multicomponent crystals. D-DTTA1 in D-D, D-DTTA2 in D-D, D-LEU1 in D-D, D-LEU2 in D-D, D-DTTA1 in L-D, D-DTTA2 in L-D, L-LEU1 in L-D, L-LEU2 in L-D, from top to bottom.

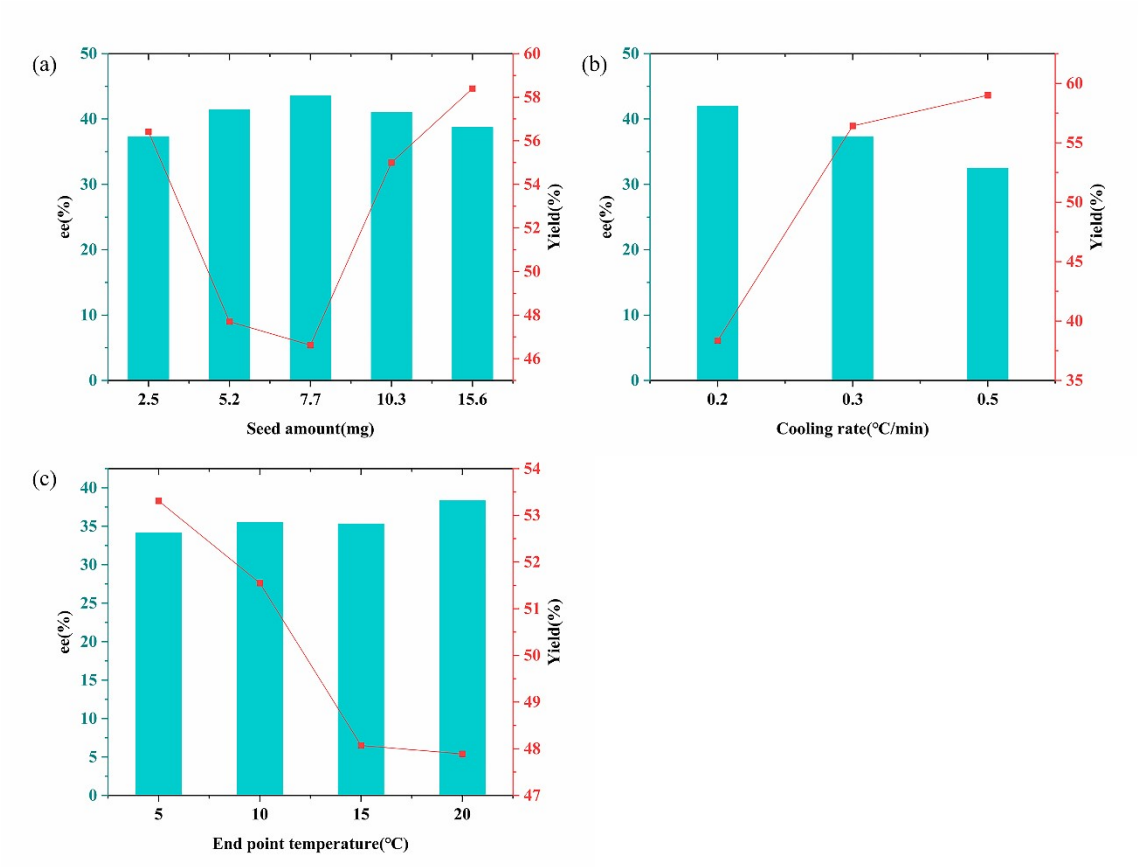

Fig. S6. The effects of seed quantity (a), cooling rate (b) and end point temperature (c) on the separation effect.

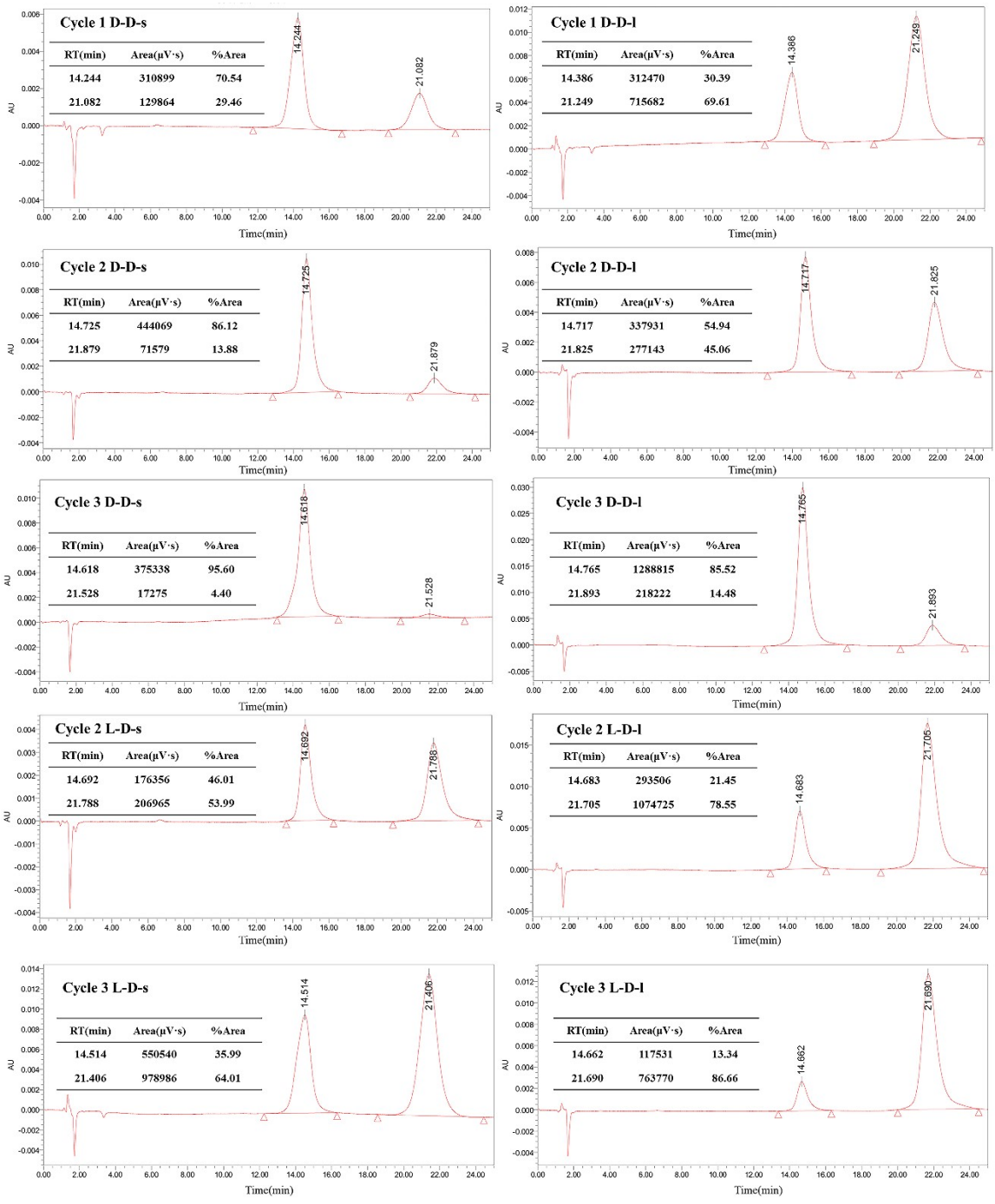

Fig. S7. HPLC data of the collected solids and liquids in each cycle.

Table S1. FT-IR stretching/bending vibration frequencies of DL-LEU, D-/L-LEU, D-DTTA, the slurry product of D-LEU with D-DTTA and the slurry product of L-LEU with D-DTTA.

Pure-/ Multi-component crystals	Stretching vibration of –NH_2 (cm^{-1})	Stretching vibration of –OH (cm^{-1})	Bending vibration of –NH_2 (cm^{-1})	Stretching vibration of –C=O (-COOH) (cm^{-1})	Stretching vibration of –C=O (RCOOR) (cm^{-1})
DL-LEU	3097	2976-2864	1615	-	-
D-/L-LEU	3052	2990-2868	1607	-	-
D-DTTA	-	3067-2920	-	1717	1732
L-LEU+D-DTTA	3177	3094-2868	1610	1703	1724
D-LEU+D-DTTA	3219	3095-2870	1610	1698	1703

Table S2. Crystallographic parameters of the prepared salts.

crystal data	D-LEU:D-DTTA :0.5H_2O[a]	L-LEU:D-DTTA :0.357CH_3OH:0.75H_2O[a]
formula	$C_{26}H_{32}NO_{10.5}$	$C_{26.36}H_{33.93}NO_{11.11}$
formula weight	526.525	542.48
T (K)	128.15	138.15
crystal system	monoclinic	monoclinic

space group	*C*2	*I*2
a (Å)	27.9114(2)	15.8758(3)
b (Å)	12.85360(10)	13.8581(3)
c (Å)	15.90080(10)	27.1887(6)
α (deg)	90	90
β (deg)	106.0490(10)	106.200(2)
γ (deg)	90	90
V (Å^3)	5482.27(7)	5744.2(2)
Z	4	8
Z'[c]	2	2
R^b	0.0385	0.0618
ρ_{calc} (g/cm^3)	1.276	1.255
μ (mm^{-1})	0.835	0.827
CCDC	2387201	2387200

[a]$\lambda_{CuK\alpha}$=1.54184. [b][I ≥ 2σ (I)]. [c]The number of synthons in an asymmetric unit.

Table S3. Hydrogen-bond metrics in crystal structures.

hydrogen bond	H···A(Å)	D···A(Å)	D–H···A(deg)
	D-D		
O6–H6···O11	1.595	2.446	169.35
O14–H14···O3	1.600	2.443	166.84
O14–H14···O4	2.635	3.265	131.23

O18–H18A···O8	1.912	2.716	159.66
N1–H1D···O4	1.862	2.723	156.91
N1–H1E···O16	2.109	2.929	149.36
N1–H1F···O12	1.812	2.719	174.59
C42–H42···O8	2.330	3.179	142.18
O20–H20···O21	1.817	2.626	161.01
N2–H2A···O9	2.022	2.877	155.95
N2–H2B···O13	1.849	2.733	163.42
N2–H2C···O5	1.847	2.741	166.93
C48–H48···O1	2.497	3.457	160.69
	L-D		
O1–H1···O22	1.80	2.612	170
N1–H1A···014	1.88	2.771	168
N1–H1B···O5	2.41	2.923	116
N1–H1B···O10	2.07	2.938	159
N1–H1C···O1	2.42	2.752	102
N1–H1C···O2A	2.35	2.695	103
N1–H1C···O7	1.98	2.756	142
N2–H2A···O12	2.10	2.931	151
N2–H2B···O6	1.78	2.680	170
N2–H2C···O15	1.85	2.732	164
O8–H8···O15	2.58	3.300	145
O8–H8···O16	1.68	2.440	149
O13–H13···O5	1.63	2.452	165
O21–H21···O2	2.04	2.816	154
O22–H22A···O23	2.12	2.841	142
O22–H22B···O2	2.07	2.836	150
O23–H23A···O4	1.98	2.789	160
O23–H23B···O4	1.98	2.789	160
C2–H2···O20	2.56	3.473	152
C4–H4···O3	2.57	3.409	141

C8–H8A···O18	2.41	3.256	142
C11–H11A···O4	2.49	3.251	134
C11–H11B···O1A	2.14	2.50	100
C34–H34···O15	2.46	2.809	100
C34–H34···O18	2.28	2.688	103
C53–H53B···O22	2.54	3.134	119

Table S4. The mole fraction solubility of D-D and L-D from 10 ℃ to 40 ℃ (p=101.3 kPa).

T/℃	D-D				L-D			
	20%	30%	40%	50%	20%	30%	40%	50%
10	6.391386E-05	9.596618E-05	0.000148	0.000528	0.000171	0.000258	0.000413	0.001411
15	7.071818E-05	0.0001112	0.000178	0.000588	0.000190	0.000321	0.000528	0.001491
20	7.911874E-05	0.0001138	0.000243	0.000609	0.000216	0.000361	0.000695	0.001805
25	9.476588E-05	0.0001605	0.000298	0.000699	0.000257	0.000426	0.001003	0.002226
30	1.129880E-04	0.0001829	0.000374	0.000855	0.000315	0.000548	0.001273	0.002816
35	1.398997E-04	0.0002134	0.000479	0.001010	0.000419	0.000669	0.001470	0.003174
40	1.795380E-04	0.0002585	0.000545	0.001233	0.000517	0.000807	0.001668	0.004364

Table S5. Atomic topological path parameters at bond critical points in D-D.

H-bond	bond (Å)	ρ (a.u.)	$\Delta^2\rho$ (a.u.)	G (a.u.)	V (a.u.)	H (a.u.)	E_H (kcal/mol)	type	E_H on average (kcal/mol)
N2–H2A···O9	0.910	0.0245	0.0996	0.0262	-0.0276	-0.0013	-4.7156	Moderate hydrogen bond interaction	-7.2698
N1-H1F···O12	0.910	0.0402	0.1236	0.0409	-0.0510	-0.0100	-8.2180		
N2-H2B···O13	0.910	0.0359	0.1262	0.0388	-0.0459	-0.0072	-7.2695		
O14-H14···O3	0.858	0.0655	0.1697	0.0667	-0.0910	-0.0243	-13.8689		
N1-H1D···O4	0.910	0.0364	0.1261	0.0388	-0.0462	-0.0073	-7.3769		
N2-H2C···O5	0.910	0.0384	0.1203	0.0390	-0.0479	-0.0089	-7.8292		
O18-H18A···O8	0.840	0.0274	0.1324	0.0348	-0.0365	-0.0017	-5.3645		
N1-H1E···O16	0.910	0.0191	0.0928	0.0220	-0.0209	0.0012	-3.5160	Weak hydrogen bond interaction	

Table S6. Atomic topological path parameters at bond critical points in L-D.

H-bond	bond (Å)	ρ (a.u.)	$\Delta^2\rho$ (a.u.)	G (a.u.)	V (a.u.)	H (a.u.)	E_H (kcal/mol)	type	E_H on average (kcal/mol)
N1-H1C···O7	0.909	0.0254	0.1216	0.0310	-0.0317	-0.0007	-4.9232	Moderate hydrogen bond interaction	-6.8850
N2-H2B···O6	0.910	0.0427	0.1328	0.0445	-0.0558	-0.0113	-8.7875		
O13-H13···O5	0.840	0.0613	0.1809	0.0666	-0.0879	-0.0213	-12.9352		
N1-H1A···O14	0.909	0.0347	0.1232	0.0373	-0.0438	-0.0065	-7.0053		
N2-H2C···O15	0.910	0.0382	0.1189	0.0386	-0.0475	-0.0089	-7.7821		
N2-H2A···O12	0.910	0.0175	0.0951	0.0219	-0.0201	0.0018	-3.1660	Weak hydrogen	

N1-H1B···O10	0.911	0.0194	0.0988	0.0237	-0.0226	0.0010	-3.5957	bond interaction

Table S7. Binding energies of D-DTTA with chiral LEU molecules.

Pure-/Multi-component crystals	Binding energy (kcal/mol)	Binding energy on average (kcal/mol)
DL-LEU	-58.49	-58.49
D-LEU1_D-DTTA1	-110.99	-131.02
D-LEU2_D-DTTA2	-151.05	
L-LEU1_D-DTTA1	-114.58	-120.09
L-LEU2_D-DTTA2	-125.60	

Table S8. Solvation Free Energy of D-D and L-D.

Multi-component crystals	ΔG_{Ideal} (kcal/mol)	ΔG_{vdw} (kcal/mol)	ΔG_{ele} (kcal/mol)	ΔG_{solv} (kcal/mol)	ΔG_{solv} on average (kcal/mol)
D-LEU1_D-DTTA1	62.132	0.216	-103.802	-41.455	-38.205
D-LEU2_D-DTTA2	61.778	6.256	-102.989	-34.955	
L-LEU1_D-DTTA1	59.185	0.932	-104.077	-43.960	-42.336
L-LEU2_D-DTTA2	61.807	1.758	-104.277	-40.712	

Screening of experimental conditions for resolution:

The effects of seed amount, cooling rate and end point temperature on the separation

effect were investigated. When the seed amount increased from 2.5 mg to 7.7 mg, the *ee* value increased and the yield decreased. This is because after the addition of seed, the crystal growth surface area will increase, and the crystal formation barrier will be further reduced, which will cause the solid phase that is homochiral with the seed to precipitate continuously over a period of time. The more seed amount, the more the surface of the crystal can be attached, and the more D-D precipitation. When the seed amount increased from 7.7 mg to 15.6 mg, the *ee* value decreased and the yield increased. This is because too much crystal growth surface will accelerate the rate of nucleation, resulting in D-D and L-D precipitation at the same time, but lead to a decline in *ee* value. Generally speaking, the higher the *ee* value, the lower the yield. The seed amount of 10.3 mg was selected. In this case, the *ee* value differs little from the maximum *ee* value, while retaining the high yield (Fig. S6a).

With the increase of cooling rate, the *ee* value decreased and the yield increased. The faster the cooling rate, the larger the nucleation driving force, the faster the nucleation rate, resulting in the simultaneous precipitation of D-D and L-D and the decrease of *ee* value. In order to ensure high *ee* value and high yield at the same time, we chose a median value of 0.3 ℃/min (Fig. S6b).

With the increase of the end point temperature, the *ee* value increased and the yield decreased. Compared with D-D, the solubility of L-D is more sensitive to temperature changes. The lower the end point temperature is, the L-D precipitation amount increases significantly, and the D-D precipitation amount does not change much, so the *ee* value correspondingly decreases. The lower the end point temperature, the smaller the solubility of D-D and L-D, and the higher the yield. In order to ensure high *ee* value and high yield at the same time, and considering that further cooling crystallization should be carried out in the future, 10 ℃ was chosen (Fig. S6c).

Specific conditions of multiple cycle crystallization process:

In the cycle 1 step of D-D, DL-LEU (1 mmol) and D-DTTA (1 mmol) were dissolved in 20 mL MeOH/H_2O at 2:3 (v/v). Subsequently, 10.3 mg D-D seed was added at 50 ℃, cooled to 10 ℃ at a cooling rate of 0.3 ℃/min, and filtered to obtain solid and mother liquor. In the cycle 2 step of D-D, the solid product obtained from cycle 1 was re-dissolved in 15 mL MeOH/H_2O at 2:3 (v/v). Other conditions remain the same as cycle 1. In the cycle 3 step of D-D, the solid product obtained from cycle 2 was re-dissolved in 10 mL MeOH/H_2O at 2:3 (v/v). The remaining conditions are consistent with cycle 1 and the final D-D product is obtained. However, the L-D products can be obtained by two cooling operations from the mother liquor generated in cycle 1 of D-D. The first cooling progress involves lowering the temperature of the mother liquor from 10 ℃ to 7 ℃ at a cooling rate of 0.3 ℃/min, while simultaneously collecting any solid particles that have formed (cycle 2 of L-D). This step also yields a new filtrate. Subsequently, the second cooling process involves further reducing the temperature of the newly obtained filtrate to 3 ℃ to obtain the final L-D product (cycle 3 of L-D).